



We provide custom laboratory and pilot equipment  
to printed electronics research & industry

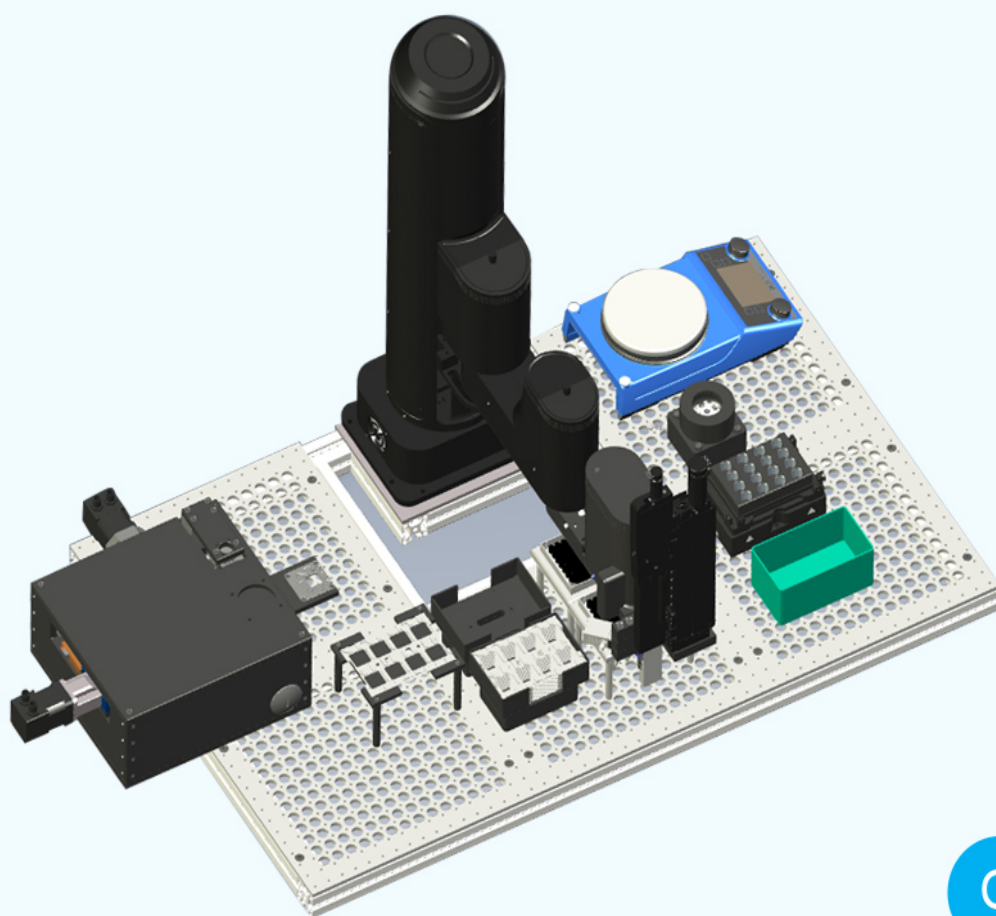
# SpinBot One

*a fully automated, customizable spin-coating robot*

- **Graphical user interface**  
to control deposition process
- **Automated processing**  
of 100s of substrates
- 1 substrate per minute using  
**multiple spincoaters in parallel**
- Full **process control** and  
reproducibility
- **Database capability**  
storage of process parameters and  
measurement results per sample

## Ready for

- **glovebox integration**
- integration of  
**characterization tools**
- **process integration to  
full devices** with  
electronic measurement  
tools and compatible to  
evaporation units



[Click to find out more](#)

 **SCIPRIOS**

*Innovative automated scientific solutions*

# Direct observation of the chemical transformations in BiVO<sub>4</sub> photoanodes upon prolonged light-aging treatments

Ramón Arcas,<sup>[a]</sup> Drialys Cardenas-Morcoso,<sup>[b]</sup> Maria Chiara Spadaro,<sup>[c]</sup> Miguel García-Tecedor,<sup>[d]</sup> Camilo A. Mesa,<sup>\*[a]</sup> Jordi Arbiol,<sup>[c,e]</sup> Francisco Fabregat-Santiago,<sup>[a]</sup> Sixto Giménez,<sup>\*[a]</sup> and Elena Mas-Marzá,<sup>\*[a]</sup>

[a] R.Arcas, C.A.Mesa, S.Giménez, F.Fabregat-Santiago, E.Mas-Marzá  
Institute of Advanced Materials (INAM) Universitat Jaume I  
Av. Sos Baynat, s/n, 12006, Castelló, (Spain)  
E-mail: cmesa@uji.es, sjulia@uji.es, emas@uji.es

[b] D. Cardenas-Morcoso  
Material Research and Technology (MRT) Department  
Luxembourg Institute of Science and Technology (LIST)  
41 Rue du Brill L-4422 Belvaux, (Luxembourg)

[c] M.C.Spadaro, J.Arbiol  
Catalan Institute of Nanoscience and Nanotechnology (ICN2), CSIC and BIST  
Campus UAB, Bellaterra, Barcelona, Catalonia, 08193, (Spain)

[d] M.García-Tecedor  
Unidad de Procesos Fotoactivados  
Instituto IMDEA Energía  
Avda. Ramón de la Sagra, 3 Parque Tecnológico de Móstoles E-28935 Móstoles, Madrid, (Spain)

[e] J.Arbiol  
ICREA  
Pg. Lluís Companys 23, 08010 Barcelona, Catalonia, (Spain).

Supporting information for this article is given via a link at the end of the document.

**Abstract:** Exposing BiVO<sub>4</sub> photoanodes to light-aging treatments is known to produce a significant photocurrent enhancement. Until now, the interpretation given to this phenomenon has been associated to the formation of oxygen vacancies and little has been reported about chemical changes in the material. Here, we demonstrate the chemical segregation of Bi species toward the surface upon light-aging treatment, which takes place with the concomitant formation of intra-band gap states associated to the oxygen vacancies. We further demonstrate that these intra-band gap states are photoactive and generate photocurrent under infra-red excitation. These results highlight the importance of understanding light-induced effects while employing multinary metal oxide photoelectrodes.

## Introduction

Photoelectrocatalysis (PEC) has emerged as an attractive route to store solar energy involving photoelectro-oxidation and photoelectro-reduction processes. To date, most of the PEC applications developed have been mainly focused either on water splitting to obtain molecular hydrogen<sup>[1]</sup> or on the reduction of CO<sub>2</sub> to C1 and C2 derivatives.<sup>[2]</sup> However, there is a growing interest to exploit alternative reactions to obtain compounds with higher added-value for the chemical industry.<sup>[3,4]</sup> Among the different transformations proposed, the PEC oxidation of primary alcohols to the corresponding aldehydes or acids has attracted significant attention.<sup>[5,6,7,17,18]</sup> BiVO<sub>4</sub> is a promising material for the development of PEC devices, mainly due to its suitable band gap (2.4 eV), which allows visible light absorption (up to 516 nm)<sup>[9]</sup> leading to a theoretical photocurrent of ~7.5 mA·cm<sup>-2</sup> under 1 sun illumination.<sup>[10]</sup> Furthermore its band structure (i.e. the position of the valence and conduction bands) leads to large photovoltages for driving organic transformations.<sup>[11–13]</sup> In contrast, the low electron mobility has been identified as the main bottleneck for the PEC performance of this material.<sup>[14,15]</sup>

The crystal structure of BiVO<sub>4</sub> is composed by Bi<sup>3+</sup> and V<sup>5+</sup> cations in coordination with O<sup>2-</sup>.<sup>[16]</sup> During structural arrangement,

the inherent formation of structural defects takes place and their concentration can be controlled by either modifying the synthetic conditions<sup>[17]</sup> or by post-synthetic treatments.<sup>[18,19]</sup> The most common defects in this material are oxygen vacancies (OV<sub>s</sub>), which are the result of removing O atoms from the lattice.<sup>[20–22]</sup> It has been shown that these OV<sub>s</sub> have a huge impact on the PEC behavior of different photoanodes for the oxygen evolution reaction (OER).<sup>[23–26]</sup> Specifically, the effect of OV<sub>s</sub> on BiVO<sub>4</sub> for OER is based on the ability of these defects to increase the bulk carrier concentration and conductivity.<sup>[27]</sup> Furthermore, an excessive density of OV<sub>s</sub> has been correlated to the decrease of performance.<sup>[28]</sup> The formation of OV<sub>s</sub> also creates intra-band gap states, mainly related to V species, where the electrons are located closer to the conduction band.<sup>[29]</sup> These new electronic states lead to enhanced light absorption and have been related to the reduction of the nearby vanadium atoms from V<sub>ov</sub><sup>5+</sup> to V<sub>ov</sub><sup>4+</sup>.<sup>[30]</sup> The attempts to directly excite these intra-band gap states associated with oxygen vacancies in BiVO<sub>4</sub> have been limited, and only a recent study by Selim *et al.* reports the use of a transient infrared light to modulate the electrical response of the photoanode.<sup>[30]</sup> Consequently, infrared excitation of OV<sub>s</sub> could clarify the role of these chemical defects on the PEC performance of BiVO<sub>4</sub>.

On the other hand, prolonged light-aging treatments have been reported to improve the PEC performance of BiVO<sub>4</sub> towards OER. Trzészniwski *et al.* showed the enhancement of both photocurrent and photovoltage for undoped and uncatalyzed BiVO<sub>4</sub> photoanodes due to a process the authors refer as photocharging (10 hours under illumination at open-circuit conditions).<sup>[31]</sup> Similar results were reported by Li *et al.* after 20 hours of curing under UV illumination.<sup>[32]</sup> In both studies, the authors attributed the increase in photocurrent to the reduction of surface recombination processes as a consequence of the decrease of the defect sites at the surface.<sup>[33]</sup> The effects of the light-aging treatments were also analyzed by Liu *et al.* using Intensity Modulated Photocurrent Spectroscopy (IMPS).<sup>[34]</sup> The authors found that after three hours of light treatment, a complex interaction between charge transfer and surface

This article has been accepted for publication and undergone full peer review but has not been through the copyediting, typesetting, pagination and proofreading process, which may lead to differences between this version and the [Version of Record](#). Please cite this article as doi: [10.1002/solr.202200132](https://doi.org/10.1002/solr.202200132).

recombination takes place, dominating the suppression of surface recombination at more positive applied potentials. More recently, Feng *et al.* reported the beneficial effects of a photoetching treatment, consisting of 10 minutes illumination at open circuit conditions. This treatment revealed that short illumination periods generates  $OV_s$  at the surface, which double the  $BiVO_4$  photocurrent due to the significant enhancement of the charge separation efficiency.<sup>[35]</sup> All these studies demonstrated that short periods (10 min – 20 hours) of light-aging preferentially modify the  $BiVO_4$  surface; however, illumination periods longer than 30 hours have not been reported yet.

Few works have tried to analyze the influence of light-aging treatments on  $BiVO_4$  using in situ spectroelectrochemical measurements. Particularly, Furet *et al.* employing a sequence of XPS, UV-Vis and XRS techniques<sup>[36]</sup> and Venugopal *et al.* using infrared spectroscopy<sup>[37]</sup> revealed a dynamic nature of the light treatments on  $BiVO_4$ /electrolyte interface, however, in these cases the effect of the electrolyte could mask the true effects of light into the material during the light-aging process.

In the present study, we report the effect of prolonged light treatments on the PEC behavior of  $BiVO_4$  photoelectrodes for the benzyl alcohol oxidation under air conditions for 48 hours. We have selected this reaction as a model platform for more complex organic transformations, opening the door to more sustainable and environmentally friendly synthetic strategies. Morphological, structural, and electrical measurements allowed us to unravel the different chemical processes taking place in the material during the light treatment and correlate them with the changes observed in PEC response. Moreover, we show for the first time, to the best of our knowledge, steady-state photocurrent generation upon continuous infra-red excitation, confirming the photoactivity of these light-induced electronic states.

## Results and Discussion

$BiVO_4$  photoanodes were prepared by electrodeposition on FTO substrates, as detailed in the Supporting Information (S.I.) and were illuminated in air to elucidate the influence of prolonged light-aging treatments for the oxidation of benzyl alcohol. Our  $BiVO_4$  photoanodes were illuminated at two different light intensities (1 and 3 suns for 1LA- $BiVO_4$  and 3LA- $BiVO_4$ , respectively) for 48 h while the other films were kept under dark conditions (Reference). All samples were tested using the operational conditions normally used to oxidize selectively benzyl alcohol to benzaldehyde.<sup>[6]</sup> A 0.1 M tetrabutylammonium perchlorate (TBAClO<sub>4</sub>) in  $CH_3CN$  solution served as non-aqueous electrolyte in order to avoid the competing water oxidation reaction. A UV filter was incorporated to the ozone free Xe lamp in order to avoid the singlet oxygen generation and the non-faradaic oxidation of benzyl alcohol,

previously reported for a similar system.<sup>[5]</sup> **Figure 1** compares the photocurrent of 1LA- $BiVO_4$  and 3LA- $BiVO_4$  to that for the Reference, showing a performance enhancement after the light-aging treatment. Similarly, the light-aging (LA) treatment produced films with higher photocurrents towards the oxygen evolution reaction (OER) as shown in S.I., **Figure S2**. The difference in the onset potential between LA and Reference sample observed for OER and not present in ROH oxidation demonstrates the higher catalytic activity of  $BiVO_4$  photoanodes towards alcohol oxidation compared to OER.

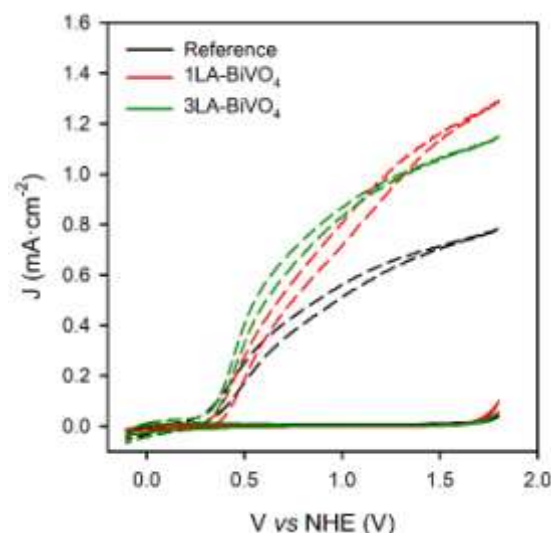


**Figure 1.** Cyclic Voltammograms of Reference (black), 1LA- $BiVO_4$  (red) and 3LA- $BiVO_4$  (green) photoanodes measured at  $20 \text{ mV}\cdot\text{s}^{-1}$  in 0.1M benzyl alcohol in acetonitrile solution with 0.1M TBAClO<sub>4</sub> in the dark (solid lines) and under illumination ( $100 \text{ mW}\cdot\text{cm}^{-2}$ ) [dashed lines].

To study the nature of the LA treatment on  $BiVO_4$ , we firstly analyzed the morphology and crystalline structure of  $BiVO_4$  by scanning electron microscopy (SEM), see **Figures 2a, 2b** and **Figure S3** in S.I. A clear change in the surface of the  $BiVO_4$  photoanodes is observed after LA. More precisely, while the Reference  $BiVO_4$  exhibits a homogenous surface (**Figure 2a**), the LA samples are characterized by the presence of several islands (region B in **Figure 2b**) formed by small nanoparticles surrounding the regular  $BiVO_4$  grains. Interestingly, EDS analysis for the different samples (**Figure 2c**), revealed that, upon LA treatment, the stoichiometric Bi/V concentration ratio of the Reference  $BiVO_4$  divides into Bi deficient (zone A in **Figure 2b**) and Bi enriched domains (zone B in **Figure 2b**). These observations evidence the morphological and chemical modification of the  $BiVO_4$  photoanodes due to LA and are directly related to the photocurrent increase shown in **Figure 1**.



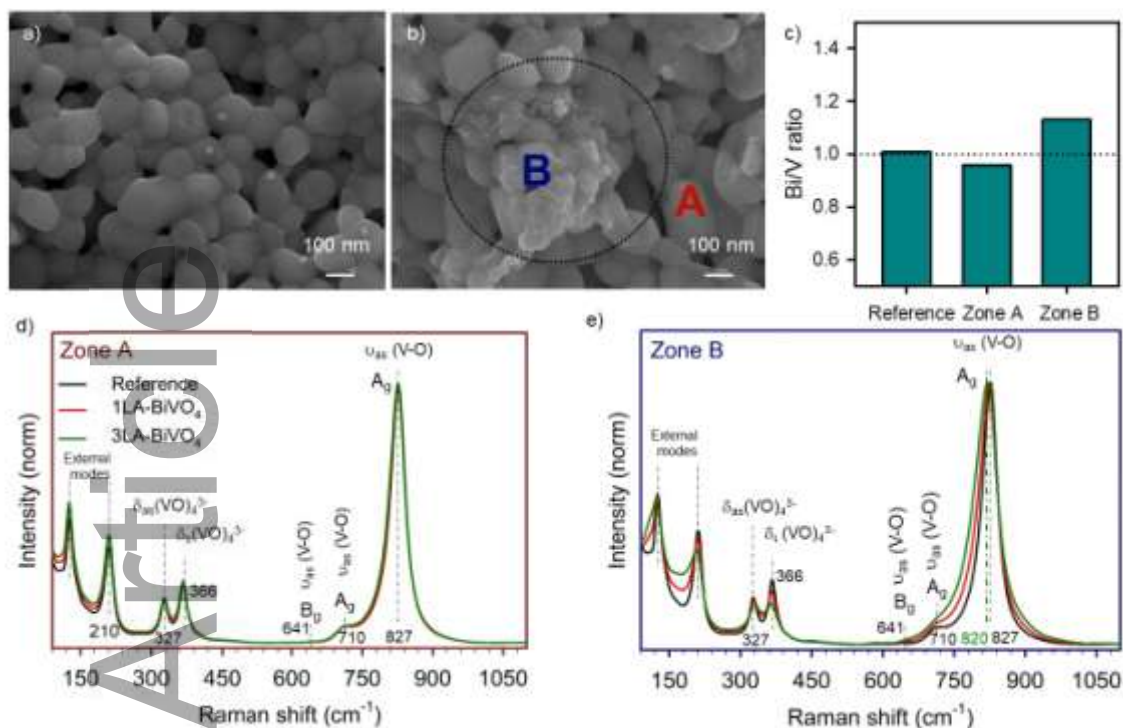


**Figure 2.** Top-view SEM images of (a) Reference and (b) 1LA-BiVO<sub>4</sub>. (c) Bi/V concentration ratio for Reference and A and B zones measured by EDS in (b). Raman spectra of (d) Zone A and (e) Zone B.

To further analyze the morphological and chemical modifications of BiVO<sub>4</sub> photoanodes induced by LA treatment, we performed Raman spectroscopy on all samples in both zones A and B in **Figure 2b**. As depicted in **Figures 2d** and **2e**, Raman bands perfectly matched with the vibrational modes of BiVO<sub>4</sub>.<sup>[38,39]</sup> Comparing the different samples, Raman bands were practically independent of LA in zone A. However, a significant band broadening is observed in zone B after LA, in particular for both the external and A<sub>g</sub> modes. This has been previously attributed to the formation of defects, such as oxygen vacancies or hydrogen impurities.<sup>[40,41]</sup> We note that that oxygen vacancies in metal oxides can also be monitored by other techniques like electron paramagnetic resonance (EPR),<sup>[42,43]</sup> cathodoluminescence,<sup>[44]</sup> transient absorption spectroscopy (TAS)<sup>[28]</sup> and spectroelectrochemistry.<sup>[45]</sup> On the other hand, XRD measurements did not evidence any relevant modification of the crystalline structure due to LA (**Figure S4** in S.I.).

We move now to investigate the morphological transformation upon light-aging by transmission electron microscopy (TEM). Indeed, compared to the homogeneous surface of the Reference BiVO<sub>4</sub> sample (**Figure 3a**), 1LA-BiVO<sub>4</sub> evidenced the development of a thin amorphous layer, as the origin of the growth of small nanoparticles, as observed in **Figure 3b**, on the BiVO<sub>4</sub> crystallites which results in a granulated surface (**Figure 3c**). Additionally, scanning transmission electron microscopy combined with electron energy loss spectroscopy (STEM-EELS) proved the increase of Bi species on the surface of BiVO<sub>4</sub> crystallites after LA (**Figure S5** in S.I.). It is apparent from **Figure 3** that

prolonged electron beam irradiation undergoes in a dramatic morphological transformation of our BiVO<sub>4</sub>. Interestingly, the migration of some atomic species from the bulk to form particles at the surface could be recorded during the electron beam irradiation (the complete sequence can be visualized in the video freely available at 10.5281/zenodo.5643642) and the final morphology presented the segregation of a significant number of nanoparticles on top of the BiVO<sub>4</sub> grains (**Figures 3c** and **3d**).

To understand the nature and composition of these aggregates, we carried out a detailed HR-TEM characterization. **Figure 3e** shows the HR-TEM image of the bulk area of a BiVO<sub>4</sub> grain. The power spectrum (Fast Fourier Transform) analysis of this area (inset in **Figure 3e**) confirms the clinobisvanite BiVO<sub>4</sub> phase I112/B (s.g. 15) oriented along its [011] zone axis. However, focusing the electron beam on the segregated nanoparticles (**Figure 3f**), the power spectrum analysis clearly indicates the presence of Bi species. The results of the power spectra analysis in different areas matched with two different Bi structures: metallic Bi with hexagonal structure (R3-MH s.g. 166) oriented along [241] and [5-51] and monoclinic Bi<sub>2</sub>O<sub>3</sub> oriented along [110] and [-114] zone axis, indicating the plausible chemical composition of this segregated particles (see **Figure S6** in S.I.).

We note that the electron beam in both SEM and TEM measurements is clearly different in wavelengths and intensities compared to sunlight (LA treatment). However, the morphology and presence of Bi-rich particles at the surface on the LA treated sample (**Figure S5** in S.I.) suggests that the localized structural modification induced by

LA is alike to that presented after electron beam irradiation, involving in both cases the segregation of Bi species.

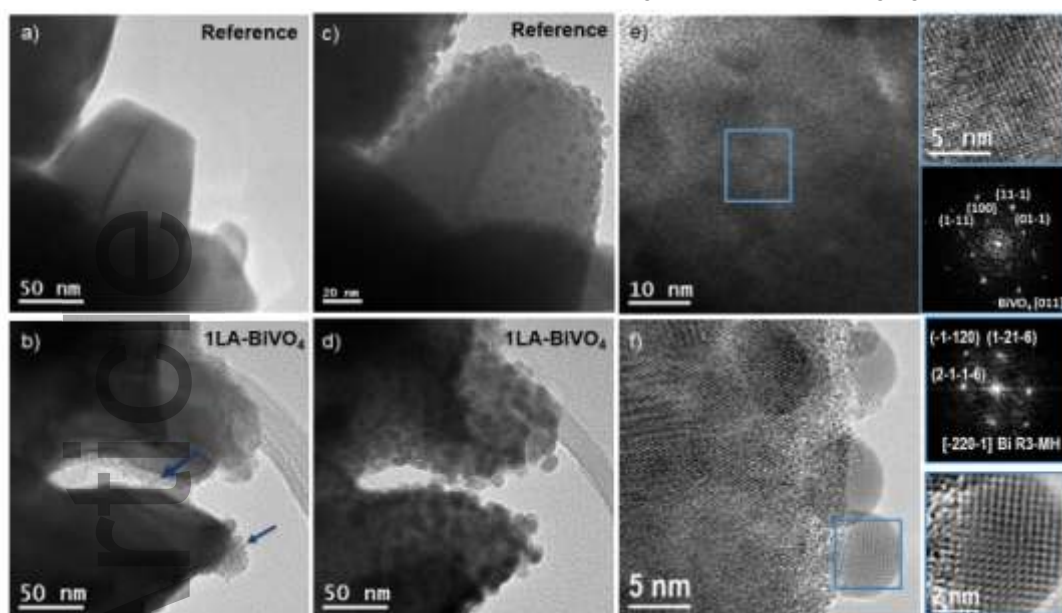


**Figure 3.** TEM images (a) - (b) before and (c) - (d) after electron beam irradiation. (a) and (c) correspond to the Reference and (b) and (d) correspond to the 1LA-BiVO<sub>4</sub>, demonstrating that the BiVO<sub>4</sub> morphology transforms during either light or electron beam irradiation. (e) and (f) HR-TEM and power spectra images of bulk and surface BiVO<sub>4</sub> grains respectively after electron beam irradiation.

Summarizing, we have shown by different spectroscopic and microscopic techniques, that LA induces OV<sub>s</sub> and a Bi segregation process. These processes have been reported previously in different studies, where BiVO<sub>4</sub> has undergone prolonged exposure to light, including light treatments studies at open circuit conditions and stability tests under operational conditions.<sup>[18,25,31,33,35,36,46]</sup> In all cases different morphological and compositional processes take place at the electrode in different electrolytes and in different structures of BiVO<sub>4</sub> converging in a higher proportion of Bi compared to V.

Now, we turn to investigate plausible mechanistic insights of the effect of LA on the functional performance of the photoanodes (as showed in **Figure 1**). To this end, we perform Impedance Spectroscopy (IS) measurements under illumination to extract Nyquist plots, at different potentials, relevant for the selective oxidation of benzyl alcohol to benzaldehyde. **Figure 4a** shows one of the experimentally obtained Nyquist plots and the selected equivalent circuit (inset) used to fit the data, which has been generally employed for different metal oxide photoanodes.<sup>[47]</sup> This equivalent circuit is commonly used to separate the contribution of bulk and surface processes in the photoanodes.<sup>[33]</sup> The elements employed are:  $R_s$  (series resistance),  $C_{\text{bulk}}$  (bulk capacitance),  $R_{\text{bulk}}$  (bulk resistance),  $R_{\text{ct}}$  (charge transfer resistance) and  $C_s$  (surface capacitance). The obtained capacitances and resistances as a function of the applied potential are reported in **Figures S7** and **S8** in S.I.

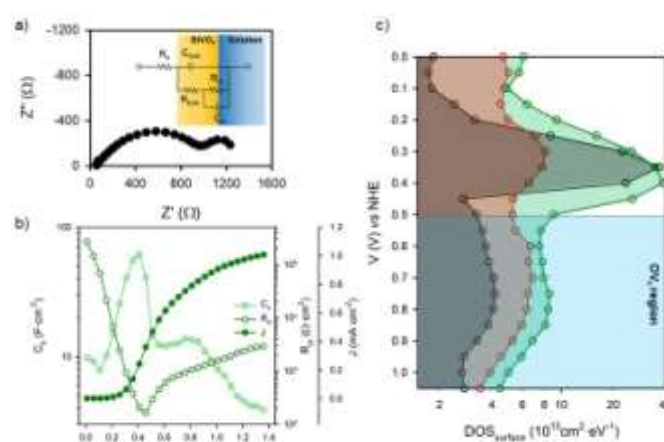


**Figure 4.** (a) Nyquist plot of Reference sample and selected equivalent circuit to fit the experimental data of the Reference and LA samples. (b) Surface capacitance ( $C_s$ ), charge transfer resistance ( $R_{\text{ct}}$ ) and photocurrent ( $J$ ) of Reference BiVO<sub>4</sub>. (c) Density of surface states as a function of applied potential. Reference (Black), 1LA-BiVO<sub>4</sub> (Red) and 3LA-BiVO<sub>4</sub> (Green). Measurements were performed under illumination, in 0.1 M benzyl alcohol oxidation conditions.

**Figures 4b** and **S7a** show the presence of two peaks at 0.35 V and 0.75 V vs NHE, for the surface capacitance ( $C_s$  light green empty circles in **Figure 4b**) of all tested samples. The peak at 0.35 V is coincident with the valley of the  $R_{\text{ct}}$  (dark green empty circles in **Figure 4b**), and both features take place at the same potential associated to the benzyl alcohol oxidation onset (dark green full cycles). A similar behavior has been already observed in different metal oxides, where a surface capacitance peak is observed just before the onset

for OER. This behavior on hematite photoanodes was assigned to charge transfer controlled by surface state charging associated to intermediate species in the reaction process.<sup>[47]</sup> Consequently, we suggest that ROH oxidation is controlled by a surface state, which dictates the hole transfer process from the electrode to the substrate. We note that this DOS is lower for the 1LA-BiVO<sub>4</sub> sample compared to the Reference material. A more detailed study of the influence of this surface capacitance on the photoelectrooxidation of benzyl alcohol remains beyond the scope of the present work.

On the other hand, the broader peak at 0.75 V vs NHE either in  $C_s$  and  $C_{bulk}$  is assigned to the  $V^{4+}/V^{5+}$  redox process, which has previously been related to the presence of  $OV_s$  in BiVO<sub>4</sub> films.<sup>[33,48,49]</sup> The presence of this peak in the reference sample suggests the intrinsic formation of this defects during the crystallization step.

Considering the  $C_s$ , the energetic distribution of these surface states,  $g(E_{Fn})$  or DOS, can be estimated by equation 1

$$C_s = q \cdot g(E_{Fn}) \quad (\text{eq. 1})$$

where  $q$  is the elementary charge ( $1.6 \times 10^{-19}$  C). **Figure 4c** shows that the calculated DOS associated to  $OV_s$  scales with the irradiation intensity, confirming the increase of the  $V^{4+}$  species during the light-aging process as mentioned previously in Raman. This result confirms the modification of the electronic environment of BiVO<sub>4</sub> during the LA. These observations are consistent with the results reported by Feng et al.<sup>[35]</sup> although, the higher concentration of  $OV_s$ , reflected on the bulk capacitance suggests that prolonged LA affects not only the bulk but also the surface of the film. Such higher  $OV_s$  concentration could also be responsible for the slightly lower photocurrent density found for the 3LA-BiVO<sub>4</sub> sample in **Figure 1**. This is supported by the detrimental role of a “too high” concentration of  $OV_s$  in BiVO<sub>4</sub> photoanodes as suggested in references,<sup>[23,41]</sup> which is also consistent with a recent report by Corby et al. in which an excessive concentration of  $OV_s$  could be negative for the PEC performance of WO<sub>3</sub> photoanodes,<sup>[28]</sup> suggesting that this effect may be general for metal oxide photoelectrodes. Furthermore, we have performed a long light aging treatment for 3 weeks (LT-1LA-BiVO<sub>4</sub>, **Figure S9** in SI), which compared to 1LA-BiVO<sub>4</sub> leads to an increased DOS of  $OV_s$ , and lower photocurrent, also in good agreement with this hypothesis. Collectively, our observations also suggest the possibility that above certain levels, Bi segregation at the surface of the BiVO<sub>4</sub> could impede the charge transfer of holes to the solution. In this case, the Bi species on the surface of BiVO<sub>4</sub> could operate as a blocking layer for surface states as shown in **Figure S7** in S.I.

Finally, to confirm the generation of new intra-band gap electronic states associated with  $OV_s$  in BiVO<sub>4</sub>, we used an infra-red (IR) continuous-wave laser as light source to extract steady-state photocurrents for the oxidation of benzyl

alcohol. Upon sub-bandgap excitation, photocurrent generation can only be due to the activation of intra-bandgap transitions in the semiconductor material (see **Figure S10** in SI). This approach, to the best of our knowledge, uses for the first-time infrared radiation (980 nm, 1.26 eV) to selectively excite the trapped electrons from the intra-bandgap states to the conduction band. **Figure 5a** shows the IR chopped chronoamperometry measurements for Reference and 3LA-BiVO<sub>4</sub> samples at 0.8 V vs NHE. The measured photocurrent stems from the excitation of the intra-bandgap states. The highest photocurrent of the 3LA-BiVO<sub>4</sub> sample is fully consistent with its increased density of intra-bandgap states, associated with  $OV_s$  (**Figure 5b**). Surprisingly, the photocurrent of the 3LA-BiVO<sub>4</sub> sample almost doubled compared to that for the Reference (from ~50 to ~90 nA cm<sup>-2</sup>). This is in excellent agreement with the equivalent increase of the DOS (from ~4 to ~8·10<sup>13</sup> cm<sup>-2</sup> eV<sup>-1</sup>) associated to  $OV_s$  (**Figure 4c**).

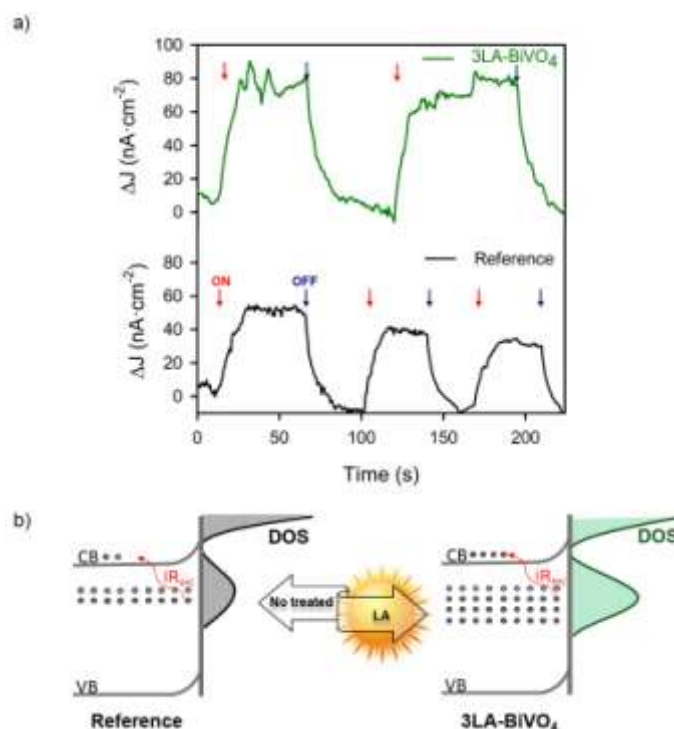


**Figure 5.** (a) Infra-red (IR) chopped chronoamperometry measurements of Reference (Black) and 3LA-BiVO<sub>4</sub> (green). (b) Band diagrams representation of the fresh and light-aged treated BiVO<sub>4</sub> samples.

We note that, although surface reduction of BiVO<sub>4</sub><sup>[50]</sup> and the increase of surface Bi species<sup>[25,51]</sup> have been previously reported, both effects have been characterized either after or during operando conditions and, consequently, they were attributed to vanadium dissolution.<sup>[37]</sup> On the contrary, the light-aging treatments and the structural characterization performed here take place in the absence of electrolyte. Therefore, the bismuth-rich surface observed is a direct consequence of the incidence of light on BiVO<sub>4</sub>. Moreover, we demonstrate the correlation between the segregation of small Bi-rich nanoparticles and the formation of new intra-bandgap states associated to oxygen vacancies. The photoactivity of these intra-

bandgap states observed under infra-red illumination opens new perspectives for the development of competitive BiVO<sub>4</sub> photoanodes.

## Conclusion

Herein, we have investigated the effect of prolonged light-aging on BiVO<sub>4</sub> photoanodes, providing a direct observation of the chemical and structural modifications after light-aging treatments. We showed that light-assisted treatments under air conditions led to the chemical transformation of the material, being more pronounced upon increased light intensity used during LA. Electrical, PEC and HR-TEM characterizations allowed assigning the chemical transformations observed to the segregation of Bi species on top of BiVO<sub>4</sub> grains, leading to the formation of new intra-bandgap states associated to oxygen vacancies. Moreover, effective photocurrent generation from these intra-bandgap states was demonstrated by infra-red light excitation, confirming the formation of oxygen vacancies during the light-aging treatment and their implications on the generation of infra-red photocurrent. These results highlight the importance of understanding the light-induced effects while employing multinary metal oxide photoelectrodes either for OER or for the synthesis of high added-value chemicals.

## Acknowledgements

The authors want to acknowledge the Ministerio de Economía y Competitividad (MINECO) from Spain (ENE2017-85087-C3-1-R and PID2020-116093RB-C41 and C43), University Jaume I (UJI-B2019-20) and Generalitat Valenciana (PROMETEO/2020/028) for financial support. Serveis Centrals d'Instrumentació Científica from UJI are also acknowledged for SEM, TEM Raman and XRD measurements. M. C. S and J. A. acknowledge funding from Generalitat de Catalunya 2017 SGR 327. ICN2 is supported by the Severo Ochoa program from Spanish MINECO (Grant No. SEV-2017-0706) and is funded by the CERCA Programme / Generalitat de Catalunya. M.C.S. has received funding from the European Union's Horizon 2020 research and innovation programme under the Marie Skłodowska-Curie grant agreement No. 754510 (PROBIST) and the Severo Ochoa programme. C.A.M acknowledges the University Jaume I for the postdoc fellowship POSDOC/2019/20 and Generalitat Valenciana for the APOSTD/2021/251 fellowship. Dr. Beatriz Julián-López and Laura Montañés are also acknowledged for their help with the measurements with the infrared laser beam and some electrodes preparation.

**Keywords:** BiVO<sub>4</sub> • light aging treatments • Bi segregation • oxygen vacancies •

- [1] M. Grätzel, *Nature* **2001**, *414*, 338–344.
- [2] B. Kumar, M. Llorente, J. Froehlich, T. Dang, A. Sathrum, C. P. Kubiak, *Annu. Rev. Phys. Chem.* **2012**, *63*, 541–569.
- [3] K. Sayama, *ACS Energy Lett.* **2018**, *3*, 1093–1101.
- [4] C. R. Lhermitte, K. Sivula, *ACS Catal.* **2019**, *9*, 2007–2017.
- [5] R. Arcas, E. Peris, E. Mas-Marzá, F. Fabregat-Santiago, *Sustain. Energy Fuels* **2021**, *5*, 956–962.
- [6] T. Li, T. Kasahara, J. He, K. E. Dettelbach, G. M. Sammis, C. P. Berlinguette, *Nat. Commun.* **2017**, *8*, 1–5.
- [7] H. G. Cha, K. S. Choi, *Nat. Chem.* **2015**, *7*, 328–333.
- [8] D. Liu, J. C. Liu, W. Cai, J. Ma, H. Bin Yang, H. Xiao, J. Li, Y. Xiong, Y. Huang, B. Liu, *Nat. Commun.* **2019**, *10*, DOI 10.1038/s41467-019-09788-5.
- [9] M. Long, W. Cai, H. Kisch, *J. Phys. Chem. C* **2008**, *112*, 548–554.
- [10] J. H. Kim, J. S. Lee, *Adv. Mater.* **2019**, *31*, 1806938.
- [11] J. K. Cooper, S. Gul, F. M. Toma, L. Chen, Y. S. Liu, J. Guo, J. W. Ager, J. Yano, I. D. Sharp, *J. Phys. Chem. C* **2015**, *119*, 2969–2974.
- [12] J. K. Cooper, S. Gul, F. M. Toma, L. Chen, P. A. Glans, J. Guo, J. W. Ager, J. Yano, I. D. Sharp, *Chem. Mater.* **2014**, *26*, 5365–5373.
- [13] Z. Zhao, Z. Li, Z. Zou, *Phys. Chem. Chem. Phys.* **2011**, *13*, 4746–4753.
- [14] F. F. Abdi, T. J. Savenije, M. M. May, B. Dam, R. Van De Krol, *J. Phys. Chem. Lett.* **2013**, *4*, 2752–2757.
- [15] M. Ziwritsch, S. Müller, H. Hempel, T. Unold, F. F. Abdi, R. van de Krol, D. Friedrich, R. Eichberger, *ACS Energy Lett.* **2016**, *1*, 888–894.
- [16] W. Luo, J. Wang, X. Zhao, Z. Zhao, Z. Li, Z. Zou, *Phys. Chem. Chem. Phys.* **2013**, *15*, 1006–1013.
- [17] J. M. Wu, Y. Chen, L. Pan, P. Wang, Y. Cui, D. C. Kong, L. Wang, X. Zhang, J. J. Zou, *Appl. Catal. B Environ.* **2018**, *221*, 187–195.
- [18] M. Lamers, S. Fiechter, D. Friedrich, F. F. Abdi, R. Van De Krol, *J. Mater. Chem. A* **2018**, *6*, 18694–18700.
- [19] B. Lamm, B. J. Trzeźniewski, H. Döscher, W. A. Smith, M. Stefiak, *ACS Energy Lett.* **2017**, *3*, 112–124.
- [20] Z. Wang, X. Mao, P. Chen, M. Xiao, S. A. Monny, S. Wang, M. Konarova, A. Du, L. Wang, *Angew. Chemie Int. Ed.* **2019**, *58*, 1030–1034.
- [21] J. Gan, X. Lu, J. Wu, S. Xie, T. Zhai, M. Yu, Z. Zhang, Y. Mao, S. C. I. Wang, Y. Shen, Y. Tong, *Sci. Rep.* **2013**, *3*, DOI 10.1038/srep01021.
- [22] M. L. Crespillo, J. T. Graham, F. Agulló-López, Y. Zhang, W. J. Weber, *Appl. Mater. Today* **2018**, *12*, 131–137.
- [23] R. Fernández-Climent, S. Giménez, M. García-Tecedor, *Sustain. Energy Fuels* **2020**, *4*, 5916–5926.
- [24] W. Wang, P. J. Strohbeen, D. Lee, C. Zhou, J. K. Kawasaki, K.-S. Choi, M. Liu, G. Gallii, *Chem. Mater.* **2020**, *32*, 2899–2909.
- [25] R. Gao, L. Wang, *Angew. Chemie Int. Ed.* **2020**, *59*, 23094–23099.
- [26] C. A. Mesa, L. Steier, B. Moss, L. Francàs, J. E. Thorne, M. Grätzel, J. R. Durrant, *J. Phys. Chem. Lett.* **2020**, *11*, 7285–7290.
- [27] H. Seo, Y. Ping, G. Gallii, *Chem. Mater.* **2018**, *30*, 7793–7802.
- [28] Sacha Corby, Laia Francàs, Andreas Kafizas, J. R. Durrant, *Chem. Sci.* **2020**, *11*, 2907–2914.
- [29] A. Walsh, Y. Yan, M. N. Huda, M. M. Al-Jassim, S.-H. Wei, *Chem. Mater.* **2009**, *21*, 547–551.
- [30] S. Selim, E. Pastor, M. García-Tecedor, M. R. Morris, L. Francàs, M. Sachs, B. Moss, S. Corby, C. A. Mesa, S. Gimenez, A. Kafizas, A. A. Bakulin, J. R. Durrant, *J. Am. Chem. Soc.* **2019**, *141*, 18791–18798.
- [31] B. J. Trzeźniewski, W. A. Smith, *J. Mater. Chem. A* **2016**, *4*, 2919–2926.
- [32] T. Li, J. He, B. Peña, C. P. Berlinguette, *Angew. Chemie - Int. Ed.* **2016**, *55*, 1769–1772.
- [33] B. J. Trzeźniewski, I. A. Digdaya, T. Nagaki, S. Ravishanker, I. Herraiz-Cardona, D. A. Vermaas, A. Longo, S. Gimenez, W. A. Smith, *Energy Environ. Sci.* **2017**, *10*, 1517–1529.
- [34] E. Y. Liu, J. E. Thorne, Y. He, D. Wang, *ACS Appl. Mater. Interfaces* **2017**, *9*, 22083–22087.
- [35] S. Feng, T. Wang, B. Liu, C. Hu, L. Li, Z. Zhao, J. Gong, *Angew. Chemie Int. Ed.* **2020**, *59*, 2044–2048.
- [36] N. J. Firet, A. Venugopal, M. A. Blommaert, C. Cavallari, C. J. Sahle, A. Longo, W. A. Smith, *Chem. Mater.* **2019**, *31*, 7453–7462.
- [37] A. Venugopal, R. Kas, K. Hau, W. A. Smith, *J. Am. Chem. Soc.* **2021**, *143*, 18581–18591.
- [38] D. Zhou, L. X. Pang, W. G. Qu, C. A. Randall, J. Guo, Z. M. Qi, T. Shao, X. Yao, *RSC Adv.* **2013**, *3*, 5009–5014.
- [39] S. Wang, P. Chen, J. H. Yun, Y. Hu, L. Wang, *Angew. Chemie - Int. Ed.* **2017**, *56*, 8500–8504.
- [40] X. Xu, Y. Xu, F. Xu, G. Jiang, J. Jian, H. Yu, E. Zhang, D. Shchukin, S. Kaskel, H. Wang, *J. Mater. Chem. A* **2020**, *8*, 1636–1645.
- [41] G. Wang, Y. Ling, X. Lu, F. Qian, Y. Tong, J. Z. Zhang, V. Lordi, C. Rocha Leao, Y. Li, *J. Phys. Chem. C* **2013**, *117*, 10957–10964.
- [42] X. Zhang, X. Du, *New J. Chem.* **2020**, *44*, 1703–1706.
- [43] R. A. Eichel, *Phys. Chem. Chem. Phys.* **2010**, *13*, 368–384.
- [44] J. D. Prades, J. Arbiol, A. Cirera, J. R. Morante, M. Avella, L. Zanotti, E. Comini, G. Faglia, G. Sberveglieri, *Sensors Actuators B Chem.* **2007**, *126*, 6–12.
- [45] L. Francàs, S. Corby, S. Selim, D. Lee, C. A. Mesa, R. Godin, E. Pastor, I. E. L. Stephens, K. S. Choi, J. R. Durrant, *Nat. Commun.* **2019**, *10*, 1–10.
- [46] D. K. Lee, K. S. Choi, *Nat. Energy* **2017**, *31*, 3, 53–60.
- [47] B. Klahr, S. Gimenez, F. Fabregat-Santiago, T. Hamann, J. Bisquert, *J. Am. Chem. Soc.* **2012**, *134*, 36.
- [48] R. Yalavarthi, R. Zbořil, P. Schmuki, A. Naldoni, Š. Kment, *J. Power Sources* **2021**, *483*, 229080.
- [49] Q. Shi, S. Murcia-López, P. Tang, C. Flox, J. R. Morante, Z. Bian, H. Wang, T. Andreu, *ACS Catal.* **2018**, *8*, 3331–3342.
- [50] Y. Hermans, S. Murcia-López, A. Klein, W. Jaegermann, *ACS Energy Lett.* **2019**, *4*, 2522–2528.
- [51] F. M. Toma, J. K. Cooper, V. Kunzelmann, M. T. McDowell, J. Yu, D.

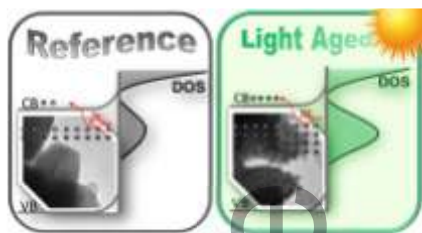


M. Larson, N. J. Borys, C. Abelyan, J. W. Beeman, K. M. Yu, J. Yang, L. Chen, M. R. Shaner, J. Spurgeon, F. A. Houle, K. A. Persson, I. D. Sharp, *Nat. Commun.* **2016**, *7*, 1–11.

Accepted Article



## Entry for the Table of Contents



Prolonged light treatments over  $\text{BiVO}_4$  photoanodes under air conditions induces Bi segregation in the surface, new intra-band gap states, as well as the formation of oxygen vacancies

Accepted Article